DOI: 10.1002/ ((please add manuscript number))
Full paper

Multiplex SERS Detection of Metabolic Alterations in Tumor Extracellular Media

Javier Plou[1,2,3], Isabel García[1,2,] Mathias Charconnet[1,4], Ianire Astobiza[3,5,] Clara García-Astrain[1], Cristiano Matricardi[6], Agustín Mihi[6], Arkaitz Carracedo[3,5,7,8], Luis M. Liz-Marzán[1,2,8]*

[1] CIC biomaGUNE, Basque Research and Technology Alliance (BRTA), Paseo de Miramón 182, 20014 Donostia - San Sebastián, Spain
[2] Biomedical Research Networking Center in Bioengineering, Biomaterials, and Nanomedicine, CIBER-BBN, 20014 Donostia - San Sebastián, Spain
[3] CIC bioGUNE, Basque Research and Technology Alliance (BRTA), 48160 Derio, Spain
[4] CIC nanoGUNE Consolider, Basque Research and Technology Alliance (BRTA), 20018 Donostia-San Sebastián, Spain
[5] Biomedical Research Networking Center in Oncology, CIBERONC, 48160 Derio, Spain
[6] Instituto de Ciencia de Materiales de Barcelona (ICMAB-CSIC), Bellaterra, Spain
[7] Biochemistry and Molecular Biology Department, University of the Basque Country (UPV/EHU), Bilbao, Spain
[8] Ikerbasque, Basque Foundation for Science, 48013 Bilbao, Spain

*To whom correspondence should be addressed: llizmarzan@cicbiomagune.es

Keywords: Surface-enhanced Raman Scattering (SERS), plasmonic substrates, tumor metabolism sensing, 3D hydrogel-based cancer cell model, tumor environment.

Abstract

The composition and intercellular interactions of tumor cells in the tissues dictate the biochemical and metabolic properties of the tumor microenvironment. The metabolic rewiring has a profound impact on the properties of the microenvironment, to an extent that monitoring such perturbations could harbor diagnostic and therapeutic relevance. Growing interest on these phenomena has inspired the development of novel technologies with sufficient sensitivity and resolution to monitor metabolic alterations in the tumor microenvironment. In this context, surface-enhanced Raman scattering (SERS) can be used for the label-free detection and imaging of diverse molecules of interest among extracellular components. We present herein the application of nanostructured plasmonic substrates comprising Au nanoparticles self-assembled as ordered superlattices, to the precise SERS detection of

selected tumor metabolites. We first demonstrate the potential of this technology through the analysis of kynurenine, a secreted immunomodulatory derivative of the tumor metabolism and the related molecules tryptophan and purine derivatives. SERS facilitates the unambiguous identification of trace metabolites and allows the multiplexed detection of their characteristic fingerprints under different conditions. Finally, we combine the effective plasmonic SERS substrate with hydrogel-based 3D cancer model, which recreate tumor microenviroment, for a real time imaging of metabolite alterations and cytotoxic effects on tumor cells.

1. Introduction

Cancer cells and the stroma create dynamic pseudo-organs that contain a unique niche with distinct biochemical and physiological properties. During the progression of the disease, tumor and stromal cells exhibit bidirectional alterations in their interaction modes and patterns of co-evolution.[1] As a result, the mutations and signaling alterations in tumor cells modify the composition of the microenvironment, whereas changes in the microenvironment can also influence the fitness of cancer cells. The reprogramming of cancer metabolism represents a biochemical process that sustains cancer growth and proliferation, while also exerting a profound influence in the tumor microenvironment.[2,3,4] Several lines of evidence support the notion that symbiotic and competitive mechanisms exist, stemming from distinct metabolite-based communication, which support tumor growth and hinder antitumor immunity. Consequently, the assessment of tumor-secreted metabolites becomes instrumental for monitoring the response of tumors upon therapeutic challenges, the stratification of cancer patients and the identification of novel therapeutic strategies. In this regard, imaging and fast detection of metabolites can play a critical role to accomplish these aims.[5,6,7]

Traditionally, extracellular metabolic studies have been carried out by means of colorimetric techniques, which involve the addition of chemical groups that specifically react with the molecule of interest. This method is rapid and convenient but also has significant drawbacks,

as it is invasive and does not allow the long-term simultaneous detection of multiple analytes.[8] More recently, liquid chromatography (LC)-coupled mass spectrometry (MS) has been the technique of choice for the majority of high- and low-throughput metabolic analysis, due to its robustness and multiple detection capability. However, LC-MS involves time-consuming, expensive and destructive procedures.[9] Nuclear magnetic resonance (NMR) is the other common analytical tool in metabolomics research. NMR allows quantifying most components in biological fluids with no need for elaborate sample preparation; however the sensitivity of NMR spectroscopy remains a weak point, as compared e.g. to LC-MS.[10,11] Hence, the development of alternative label-free methods to rapidly detect multiple tumor-secreted metabolites in extracellular media is required toward understanding metabolic interactions in the tumor niche.[12]

Surface-enhanced Raman scattering (SERS) spectroscopy, an optical ultrasensitive analytical method that can be applied non-invasively for label-free detection and imaging of a wide range of analytes, stands as a promising technique that fulfills several of the above mentioned requirements.[13] SERS allows the identification of vibrational fingerprints of probe molecules in contact with a plasmonic nanostructure and its sensitivity can go as far as the single-molecule level.[14] Therefore, SERS has emerged as a promising method for the detection and characterization of biological molecules in solution and within cells for cancer diagnosis.[15,16] On the one hand, on account of the complexity related to the interpretation of spectra obtained in biological media, much work has focused on comparing spectra of samples from healthy and cancer patients.[17-20] On the other hand, efforts have been made to computationally decipher the contributions of a number of analytes to the final SERS spectra.[21,22]

We report a SERS-based strategy to monitor the extracellular accumulation of metabolites relevant to tumor biology, applying a recently developed nanostructured plasmonic substrate comprising a superlattice of Au nanoparticles, as the source of enhancement for the Raman

signal from the analytes (**Scheme 1**). Our results support the potential of this technology for non-destructive and sensitive detection of metabolites in the extracellular compartment, which we demonstrate through the detection of immunomodulatory kynurenine (Kyn) and tryptophan (Trp), and the setup of a cytotoxicity assay based on the detection of purine derivatives. We then implemented this SERS-based detection system to image the accumulation of purine derivatives in cancer-on-a-chip models, thereby achieving spatiotemporal monitoring of cell death upon induction of cellular stress. The quality of the recorded SERS spectra reinforced the efficiency and versatility of the method for the label-free molecular detection of small metabolites in the extracellular medium, and its potential contribution to understanding the fluctuations of such molecules within the tumor microenvironment.

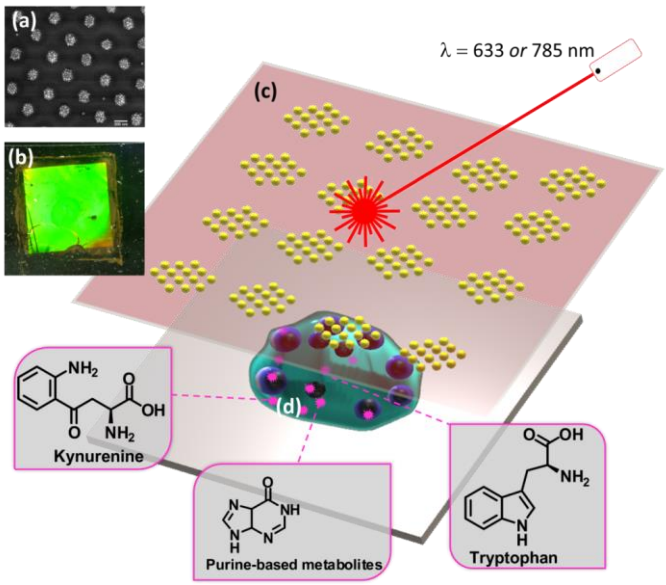

Scheme 1. Schematic illustration of the SERS-based system to detect the accumulation of metabolites in the extracellular tumor milieu. (a), (b) and (c) Nanostructured plasmonic substrate comprising a superlattice of Au nanoparticles. (d) Chemical structures of the different tumor associated metabolites accumulated in the tumoral extracellular microenvironment.

2. Results and discussions

2.1 Plasmonic substrates for SERS detection of Kynurenine and Tryptophan

We initially studied the application of SERS to identify the presence of selected metabolites, commonly secreted by cancer cells and relevant to tumor biology, including tryptophan, kynurenine and purine derivatives.[23,24] We tested two types of plasmonic substrates, which were previously optimized for the detection of bacterial Quorum Sensing signaling molecules.[25,26] Although both strategies involve the deposition of 30 nm spherical Au nanoparticles (AuNPs) on glass substrates, the different methodologies (see Methods section for detailed descriptions) result in radically different distributions of AuNPs on the substrate.[25,26] On the one hand, the standard polyelectrolyte layer-by-layer (LbL) assembly methodology was used to produce homogenous (disordered) multilayers of AuNPs on a glass cover slip (a schematic description of the fabrication is shown in **Figure S1a**). On the other hand, a recently developed template-assisted self-assembly process resulted in the formation of hierarchical nanostructured substrates, comprising square arrays of hexagonally packed AuNP clusters (**see Figure 1a**), so-called plasmonic superlattices (a graphical representation of the fabrication procedure is shown in **Figure S1b**). The different AuNP organization resulted in significant differences in the extinction spectra of the substrates. Comparison of the spectra (normalized to the amount of gold) for both substrates revealed that the plasmonic superlattices support a sharp resonance around 760 nm, which closely matched the 785 nm SERS excitation laser wavelength, whereas LbL films displayed a much broader extinction band, while retaining a maximum within the same wavelength range (**Figure 1b**). This significant difference is due to Rayleigh anomalies occurring in periodic plasmonic structures, as previously reported.[27] This physical phenomenon occurs when in-plane diffracted waves interact with the gold nanoparticle clusters, resulting in an enhancement of the plasmon resonance around the wavelength of the Rayleigh anomaly, which also results in an additional increase of the electric near-field within each AuNP cluster (**Figure S2**). This event, also

known as lattice plasmon resonance, can be modulated into a desired wavelength range, by varying the lattice period of the plasmonic substrate. We selected a lattice parameter (L) of 500 nm to obtain a lattice plasmon resonance around 760 nm, i.e. closely matching the excitation laser wavelength of 785 nm for SERS experiments (**Figure S3**).

Shown in **Figure 1c** are Raman and SERS spectra of commercial Kyn and Trp, recorded both in the solid state and in solution. For SERS measurements, 100 µL of a 100 µM analyte solution was deposited on the corresponding nanostructured plasmonic substrate and subsequently illuminated with the 785 nm laser. The obtained results show that the Kyn SERS spectrum is dominated by a narrow peak at 560 cm^{-1}, corresponding to the aminophenyl group.[28] The SERS spectrum of Trp was characterized by broader peaks, including one localized around 760 cm^{-1}, which corresponds to the indole moiety.[29] SERS spectra of commercial Kyn and Trp at different concentrations were then collected and compared to the SERS spectrum of phosphate buffered saline (PBS) on the same plasmonic support, used as a blank. For both analytes, 1µM was the lowest concentration that could be safely distinguished from the blank. This limit of detection is sufficient for the detection of both metabolites in the extracellular space ($\approx$ 10-100 µM).[30] In addition, we observed a correlation between metabolite concentration and SERS intensity within this concentration range **(see Figure S4a)**.

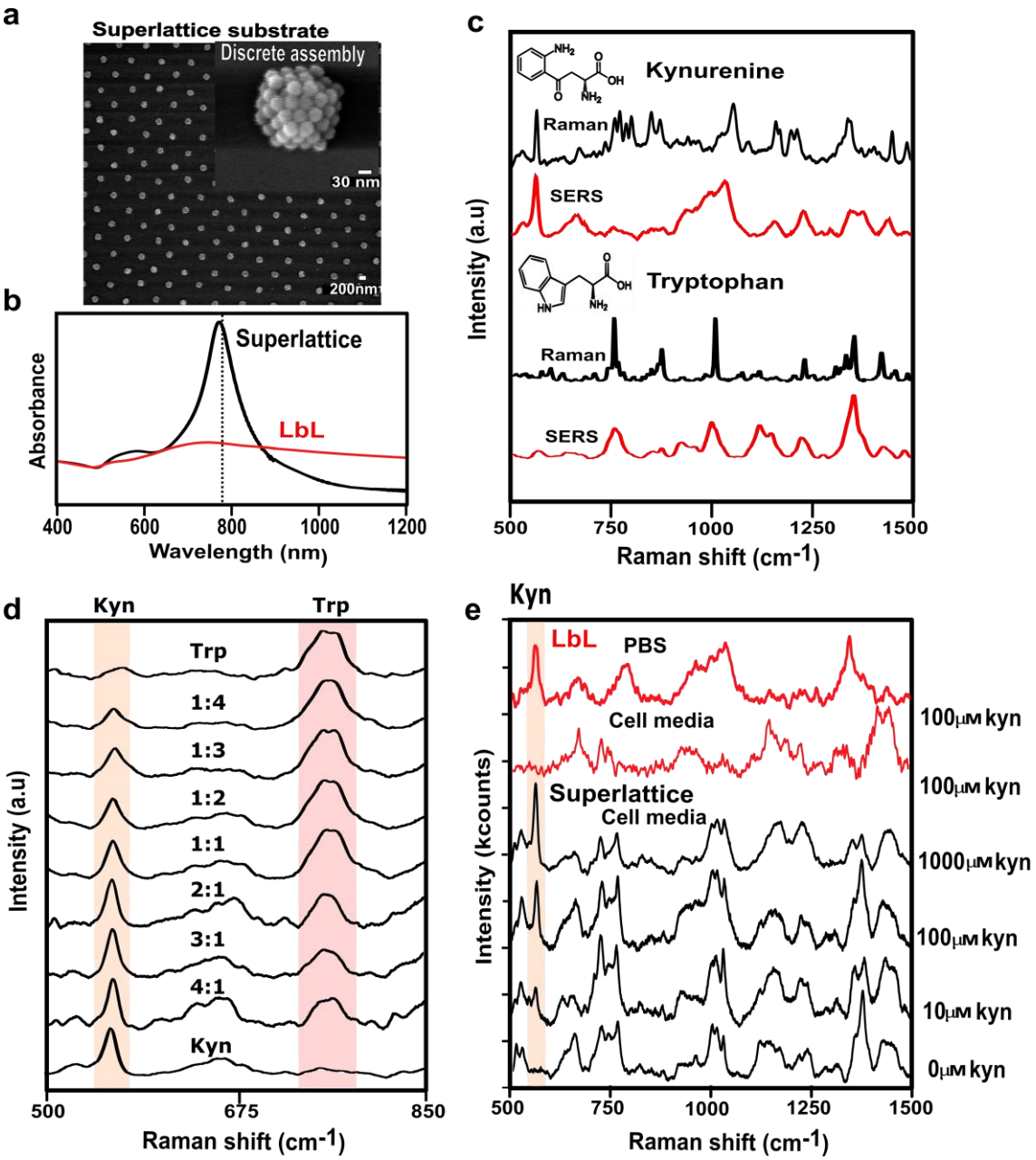

Figure 1. a) Representative SEM image of the organized discrete assemblies of Au nanospheres in the superlattice substrate. The inset shows the structure of a representative NP assembly. b) Vis-NIR spectra, normalized to 400 nm, for both LbL and superlattice plasmonic substrates; the vertical line indicates the excitation wavelength used for SERS measurements (785 nm). c) Comparison of Raman and SERS spectra for kynurenine (Kyn) and tryptophan (Trp), measured in the solid state (black) and in 100 μM aqueous solution deposited on a superlattice substrate (red). All measurements were performed with a 50× objective, 10 s acquisition time, maximum power of the 785 nm laser 295.13 kW cm^{-2}. d) SERS spectra of kynurenine-tryptophan mixtures with different ratios; the kynurenine characteristic peak (560 cm^{-1}) is highlighted with an orange bar, the tryptophan peak (760 cm^{-1}) with a pink bar. e) SERS spectra from different plasmonic substrates, in PBS and cell media. The presence of cell media masks the signal of the kynurenine peak at 560 cm^{-1} (orange label) and prevents its quantification in LbL substrates.

The concentrations of both selected metabolites (Kyn and Trp) in extracellular media are regulated by IDO-1 enzyme, which is over-expressed in many tumor cell types. More

specifically, IDO-1 utilizes Trp to generate Kyn, thereby impoverishing the extracellular milieu in Trp and enriching it in Kyn **(Figure S4c**). This metabolic reaction has recently attracted much attention as a consequence of the association of high Kyn/Trp ratios in plasma from cancer individuals with poor patient prognosis.[31,32] In this context, we hypothesized that the implementation of a SERS detection scheme would provide an efficient methodology to monitor Kyn/Trp ratio in the extracellular environment, and in turn for the extrapolation of IDO-1 expression. For the initial determination of the Kyn/Trp ratio, the metabolites were co-incubated on superlattice substrates at varying relative concentrations. The characteristic SERS spectral features allow simultaneous determination of both metabolites, using the peak at 560 cm^{-1} for Kyn and that at 760 cm^{-1} for Trp, which are sufficiently well differentiated in spite of being a closely related pair of analytes. As shown in **Figure 1d**, the relative contribution of the selected fingerprint peaks gradually changed for different Kyn/Trp ratios. We can therefore estimate the Kyn/Trp ratio from the corresponding ratio between the SERS intensities of these main peaks. Our results confirmed that semi-quantitative monitoring of both analytes could be achieved for the selected tryptophan-kynurenine combinations (**Figure S4d**). Similar results for Kyn and Trp detection could be achieved using LbL multilayer substrates (**Figure S5**).

It should be noted that the aforementioned experiments were performed in simple metabolite solutions, far from the complexity found in real biofluids, where Kyn and Trp are a minor fraction and the likelihood of interference using SERS would significantly increase. In fact, detection of specific metabolites within complex environments is considered as one of the major challenges to be addressed by optical-based detection systems.[12,33] Although both plasmonic substrates were sufficiently efficient to identify Kyn in phosphate buffered saline (PBS), when we incubated varying concentrations of Kyn in cell media, discrepancies were observed between the spectra obtained using both substrates (see **Figure S6a, S6b**). As shown

in **Figure 1e**, only the superlattice substrate was reliable toward the detection of kynurenine in complex media, whereas no significant bands at 560 cm^{-1} could be identified using LBL substrates. This result is in agreement with the improved plasmonic performance, based on the excitation of lattice plasmon modes when exciting the superlattice at 785 nm. Importantly, when we employed plasmonic superlattice structures, the detection of kynurenine was confirmed at 10 µM in cell media.

2.2 Analysis of the metabolic alterations induced by IDO-1 expressing cells

We therefore selected the nanostructured plasmonic superlattice substrates to study extracellular metabolic alterations, as well as the activity of IDO-1 in tumor cells under different conditions. For this purpose, HeLa cells were challenged with interferon-gamma (IFN-ϒ) as a suitable model to activate IDO-1 expression.[30,34] HeLa cells treated with IFN-ϒ (100 ng/mL) consistently induced IDO-1 expression (**Figure S7**). Cells challenged with IFN-ϒ were rinsed and fresh media was supplemented with varying Trp concentration, in order to monitor its conversion to Kyn. Of note, media was also supplemented with 10 µM of hemin, a cofactor of IDO-1 enzyme, which is necessary for the tryptophan catalytic conversion.[35,36] HLPC-MS-based metabolic measurements of Trp and Kyn confirmed the IFN-ϒ-elicited conversion of Trp to Kyn, due to induced IDO-1 expression (**Figure S8, S9, S10, S11**). As shown in **Figure 2a**, consistent differences were observed between spectra recorded from various cell supernatants. IFN-ϒ treatment of HeLa cells resulted in the detection of a SERS signal indicating the presence of Kyn (560 cm^{-1}) see **Figure S12**, whereas no signal was identified in control experiments. In addition, the absence of supplemented Trp in media prevented the accumulation of Kyn, in line with the lack of IDO-1 substrate. Subsequently, we calculated the Kyn/Trp ratio as described above, resulting in data for the ratio between both metabolites (**Figure 2b**). Increasing Trp was consistently accompanied by lower Kyn SERS signal. Additionally, SERS measurements allowed us to study time-dependent changes

in cell media, under the same conditions of tryptophan (100 µM) and IFN-ϒ treatment (**Figure 2c**).

As a complementary approach to promote the production of Kyn, we chose to expose HeLa cells to increasing doses of an IDO-1 co-activator analog, hemin, as a commercial analog of the heme group, a non-polypeptide unit required for the biological function of IDO-1. As shown in **Figure 2d**, hemin supplement was required for Kyn production, in agreement with its impact on the activation of IDO-1. We observed that hemin addition affected the recorded SERS profile in a dose-dependent manner, beyond the sharp signal at 560 cm^{-1}. **Figure 2e** illustrates that high hemin concentrations (100 µM) resulted in the detection of an intense SERS band at 725 cm^{-1}, commonly assigned to purine derivative metabolites.[37] We also observed an increase in cell death at high hemin concentration, which suggested a cytotoxic effect of this cofactor (**Figure S13**).[38] This cellular process drove us to speculate that both events, cell death and the release of purine derivatives, were correlated and could be investigated by SERS.

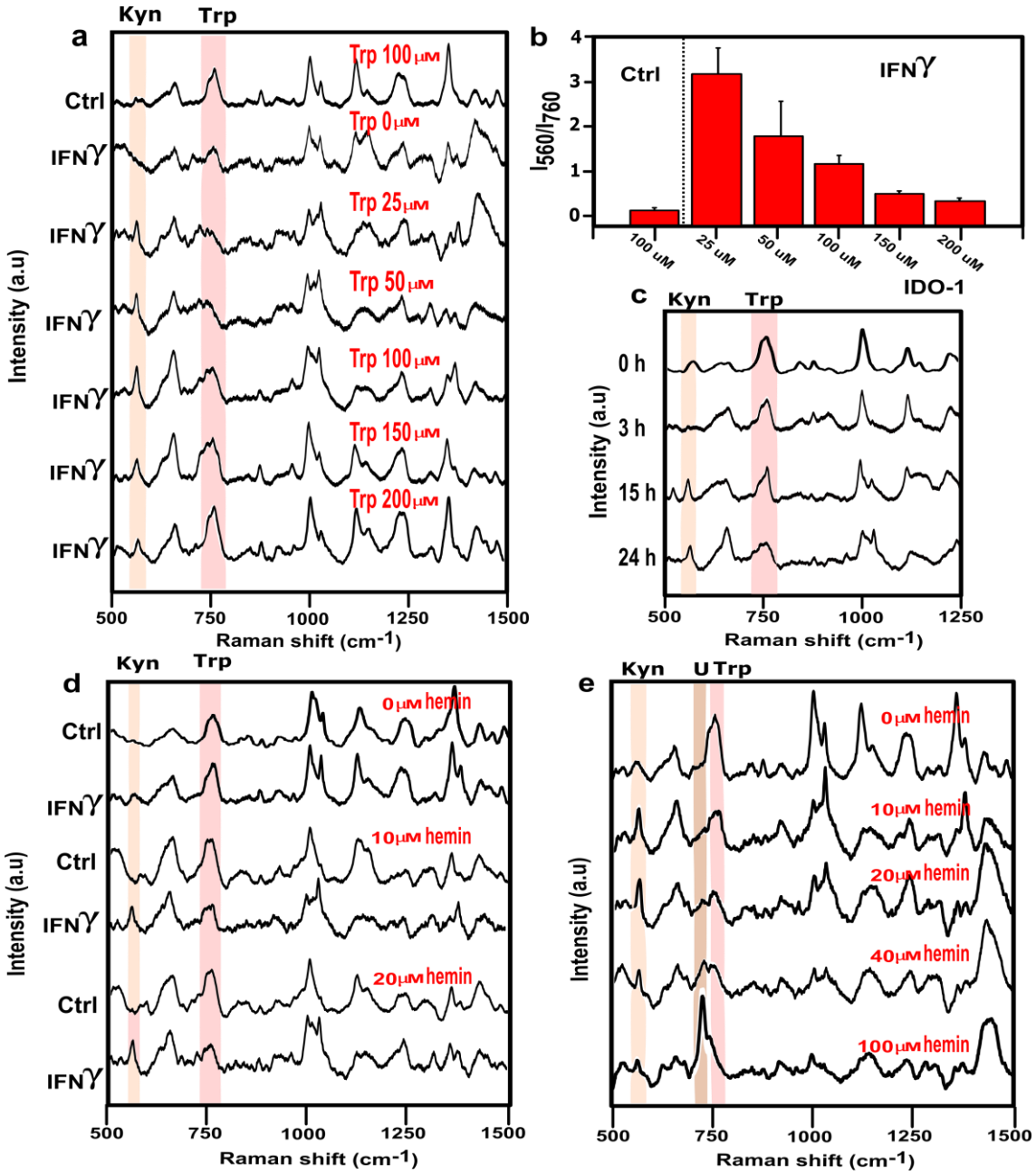

Figure 2. a) SERS spectra of cell supernatants after 24h. Cells were harvested, varying the addition of IFN-ϒ, which induces the expression of IDO-1 enzyme, and the initial tryptophan concentration. The orange bar tracks the kynurenine peak while the tryptophan signal is indicated by a pink bar. The spectra are the average spectrum of 25 measurements from a representative sample. b) Ratio between kynurenine (560 cm^{-1}) and tryptophan (760 cm^{-1}) in control and after 3 days of IFN-ϒ conditions (100ng/mL) and Trp supplementation from 25 to 200 µM, as calculated from SERS data. The error bars show the standard deviation of three independent cell assays. c) SERS spectra of cell supernatants extracted at different times. Cells were previously activated with IFN-ϒ and incubated with 100 µM of Trp. d) SERS spectra of cell supernatant obtained from cells which were incubated with 100 µM of Trp and varying addition of IFN-ϒ and hemin concentrations (0, 10, 20 µM) e) SERS spectra of cell supernatant of IFN- ϒ activated cells and incubated with 100 µM of Trp and varying concentrations of hemin (0, 10, 20, 40, 100 µM). The brown bar tracks the presence of the peak at 725 cm^{-1}, named U as an undefined event. SERS measurements were performed with a 50× objective and 10 s of acquisition time, the maximum power of the 785 nm laser was 295.13 kW cm^{-2}.

2.3 Detection of extracellular Hypoxanthine accumulation in cell death events

Recent studies put the focus on the crucial role of purine derivative metabolites within the extracellular environment and how anticancer therapies can promote the accumulation of these molecules in the extracellular milieu of tumors.[39- 42] From the unexpected results obtained in the above described experiments, we envisioned the biological value of monitoring variations of purine derivatives by SERS, to sense changes in tumor environment. Initially, we measured a number of representative purine derivative metabolites, such as ATP, adenine, adenosine, inosine and hypoxanthine (HX). The recorded SERS spectra provided a moderate distinction between adenine and hypoxanthine as shown in **Figure 3a**. In particular, a mild shift was observed in the main peak, from 735 cm^{-1} in adenine related molecules (black) to 725 cm^{-1} in hypoxanthine derivatives (red). This spectral modification can be attributed to chemical variations, more specifically the deamination process, between adenine and hypoxanthine nitrogenous bases.[43] The molecular structure of both bases (see inset in Figure 3a) reflects that adenine contains an extra amino group in the purine ring, compared to hypoxanthine.

To demonstrate that SERS can be effectively employed to detect the release of these purine bases in the extracellular milieu, we exposed HeLa cells to diverse stress conditions, such as high concentrations of hydrogen peroxide and Staurosporine, which are well-defined inducers of apoptosis.[44] We measured the SERS spectra from cell supernatants after 24 hours under the selected conditions. We found that, indeed, SERS signals corresponding to the accumulation of purine derivatives were markedly altered under stress conditions, in an analogous manner as previously observed in hemin addition experiments (**Figure 3b).** We finally tested whether drug concentration would correlate with the intensity of the peak at 725 cm^{-1}, which can be partly attributed to HX (**Figure S14**). From the results displayed in **Figure 3c**, we observed a rising trend, which reached a maximum at 10 μM of Staurosporine, when a high percentage of the cells were dead (**Figure S15a**). Interestingly, the percentage of cell

death obtained from cell viability assays showed a good correlation with the trend observed from the SERS intensity of the peak at 725 cm^{-1} (**Figure S15b,c**). This similarity, together with the results obtained by HPLC-MS analysis (**Figure S16, S17**), strengthen the idea that both events are connected.

In view of the sensitivity of the results achieved through SERS detection of purine derivative metabolites, we went a step further toward the application of SERS for *in situ* sensing of different analytes in hydrogel-based cancer models. For this purpose, we designed a configurable cancer-on-a-chip system which mimicked a more physiologically relevant 3D structure of collagen,[45,46] and then explored the combination of this platform with plasmonic substrates **(Figure 3d).** We initially cultured a collagen bioink laden with HeLa cells inside printed silicone chambers, filled with cell media, up to the selected time to make SERS measurements, then, the chamber was stacked with the plasmonic substrate and illuminated with the 785 nm laser **(Figure S18).** We found that SERS signals corresponding to the accumulation of HX in the extracellular media could still be detected under stress conditions, namely 5 µM Staurosporine (**Figure 3e**). On the other hand, SERS mapping of control cells (no Staurosporine addition) did not reveal any significant signal of HX production. Interestingly, as shown in **Figure 3d**, plasmonic monitoring of HX molecules could be performed, by following the intensity of the peak at 725 cm^{-1} over large (millimeter-scale) regions of the extracellular environment, without disrupting the system. The uniformity of HX levels in the maps recorded under stress conditions indicates a suitable diffusion of HX from the hydrogel-based cancer model to the plasmonic substrate.

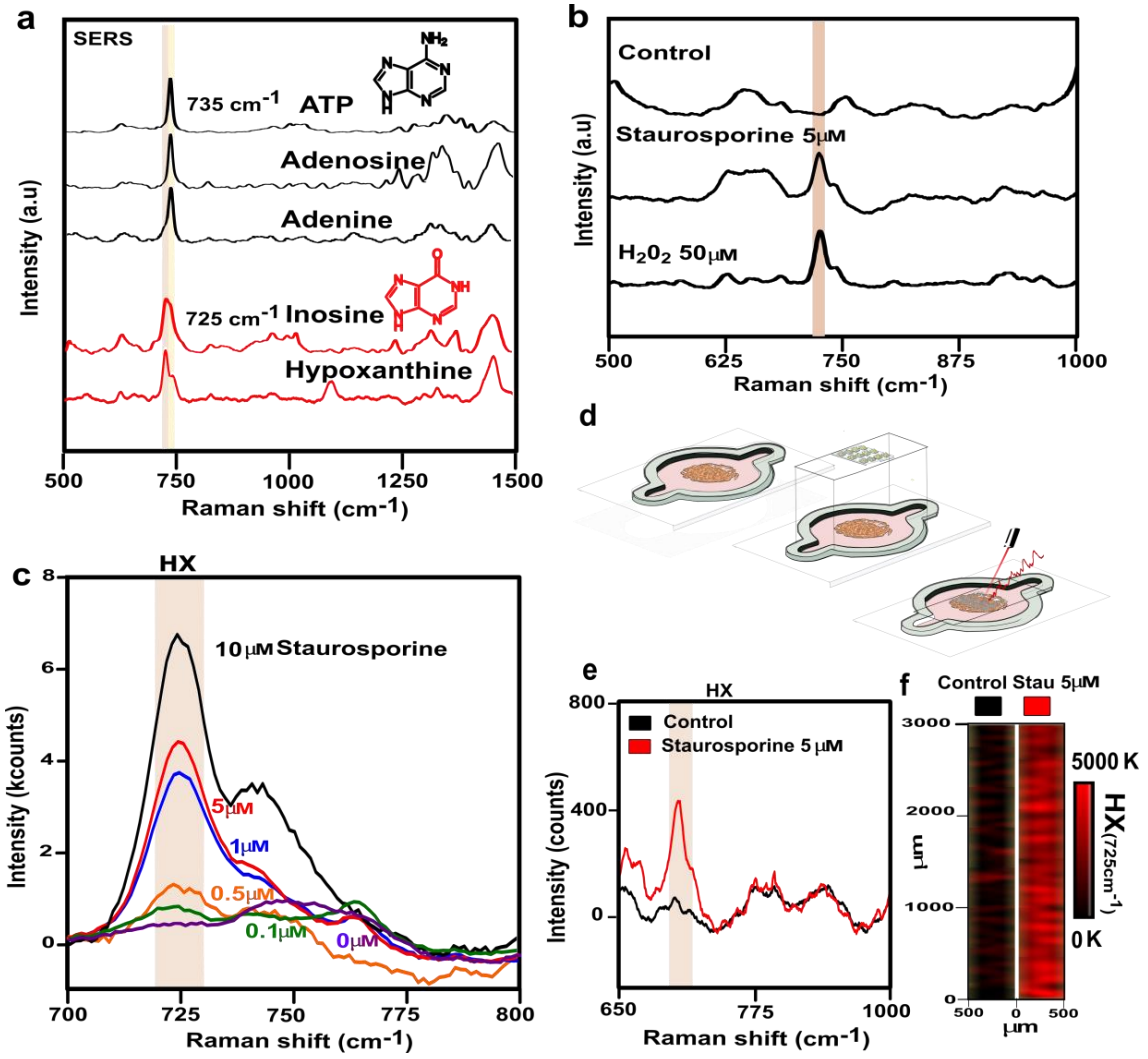

Figure 3. a) SERS spectra of adenine and hypoxanthine derivate metabolites, brown and yellow bars identify the characteristic peak of hypoxanthine (725 cm^{-1}) and adenine (735 cm^{-1}) respectively. SERS measurements were performed with a 50× objective, the maximum power of the 785 nm laser was 295.13 kW cm^{-2} and 10 s of acquisition time. b) SERS spectra of cell supernatants extracted after 24 hours of cell culture, under different stress conditions. The contribution to the averaged spectra of adenine and hypoxanthine related molecules is highlighted by brown and yellow bars, respectively. The spectra are the average of 25 measurements on a representative sample. c) SERS spectra of cell supernatants after 24 hours of cell incubation with different Staurosporine concentrations. The spectra are the average of 25 measurements on a representative sample. d) Schematic view of the methodology used to combine a 3D cell culture inside a silicon chamber with SERS measurements. e) Average of SERS spectra recorded under different Staurosporine concentrations. f) SERS mapping (725 cm^{-1}) acquired with excitation laser wavelength of 785 nm,10× objective and a laser power of 115.95 kW cm^{-2}, for 5 s.

2.4 Imaging of hemin cytotoxic effect in 3D cell culture

We finally exploited the cancer-on-a-chip system for the *in situ* sensing of hemin concentrations and its cytotoxic effect by SERS. Hemin molecules exhibit a broad absorption band in the visible, which drops at 700 nm, so that illumination of an aqueous solution of

commercial hemin with a 633 nm laser leads to resonant Raman conditions. Therefore, SERRS rather than SERS spectra of hemin were recorded **(Figure S19).** Our choice of plasmonic superlattices as SERS substrates offers the possibility of varying the lattice parameter to obtain a lattice plasmon mode in resonance with the 633 nm laser (**Figure 4a**).[27] The results plotted in **Figure 4b** illustrate the achieved improvement in hemin detection when the lattice plasmon wavelength of the substrate matched the 633 nm excitation laser, through the SERRS pyrrole ring vibration signal of hemin. As a consequence, we reconfigured the system over the course of the experimental protocol (watch **Video1**, **Video2**), alternating plasmonic substrates with different lattice parameters (L = 400 nm or 500 nm), so as to efficiently match the different laser wavelengths (633 nm and 785 nm), thereby being able to detect both hemin and HX.

We first challenged the 3D cell cultures with two different hemin concentrations (75, 100 µM) and monitored them in the cancer-on-a-chip platform by SERRS (633 nm laser; L = 400nm), as shown in **Figure 4c** and in the SERS/SERRS spectra shown in **Figure S20** (SI)**.** After 24 hours, we reconfigured the system by replacing the plasmonic substrates (L=500 nm) and illuminated with the 785 nm laser. The results shown in **Figure 4d** illustrate the effect of hemin on the extracellular HX concentration, again confirming that higher hemin concentration results in higher release of HX (**Figure S21a**). Thus, we evaluated the effect of the highest hemin concentration over time. Notably, the SERS fingerprint of HX was clearly identified as early as five hours after initiating the treatment, and the signal intensity increased over time, as shown by the SERS spectra recorded at 15 and 24 h (**Figure 4e**). This indicates that hemin can have an early cytotoxic effect on cancer cells, by altering the extracellular milieu **(Figure S21b)**.

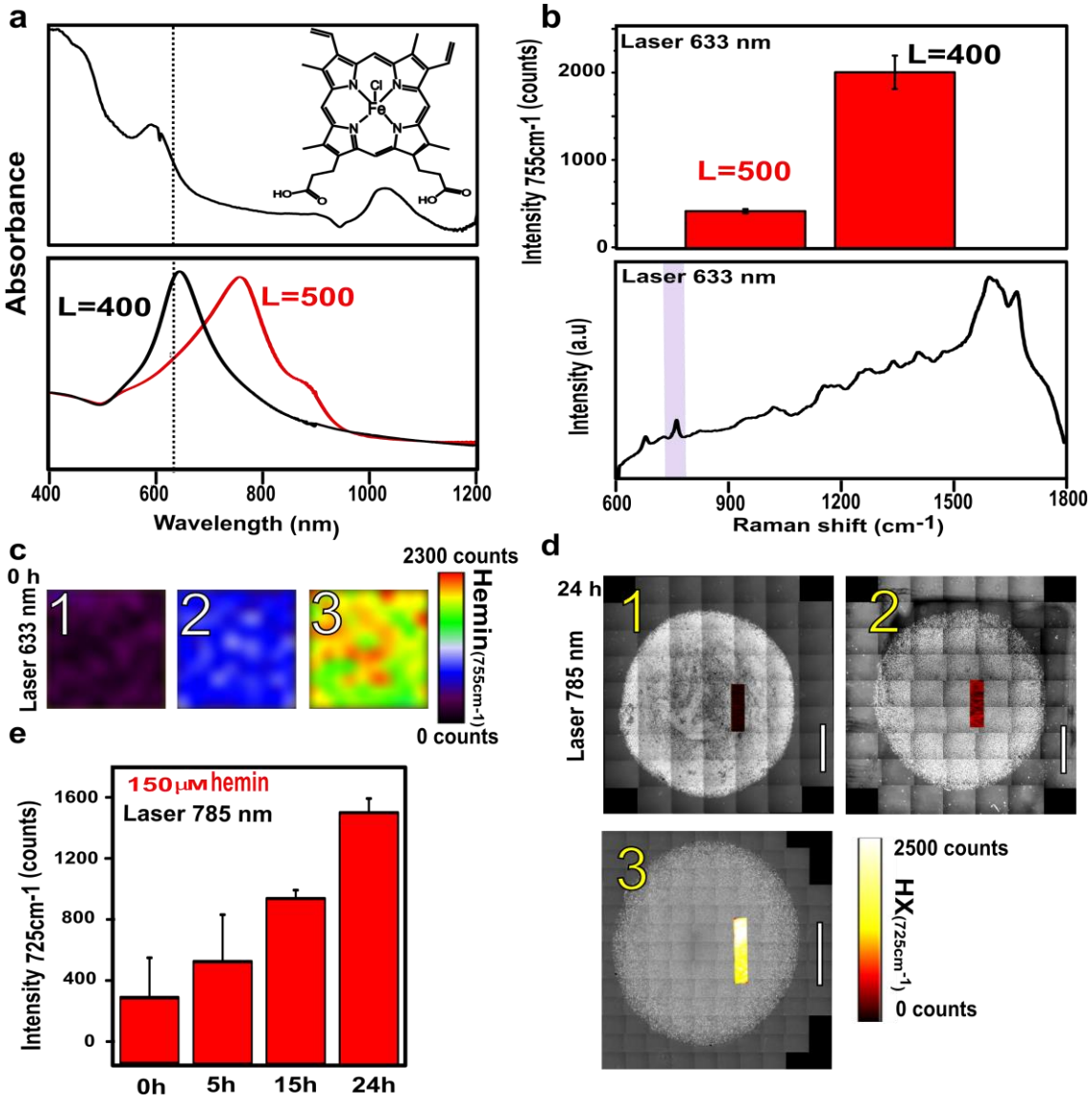

Figure 4. a) Normalized Vis-NIR spectrum and chemical structure of hemin (upper panel) and normalized Vis-NIR spectra of plasmonic superlattices with different lattice parameters, as labeled. The dotted vertical line indicates the excitation wavelength (633 nm) used for the SERRS measurements of hemin. b) SERRS spectrum of hemin and the corresponding intensities of the peak at 755 cm^{-1} (purple bar), as a function of the lattice parameter. The measurements were recorded with a 50× objective, maximum laser (633 nm) power of 51.87 kW cm^{-2} and acquisition time of 10 s. The spectrum is the average of 25 measurements. c) SERRS mapping (755 cm^{-1}) after addition of different hemin concentrations: 1 (0 µM), 2 (75 µM) and 3 (150 µM), acquired under the same conditions. d) Optical image of the hydrogel-based cancer model captured with a cell observer microscope and superimposed with the corresponding HX SERS mapping (725 cm^{-1}) of a selected area. Yellow numbers indicate different initial hemin concentrations: 1 (0 µM), 2 (75 µM) and 3 (150 µM), scale bar: 2 mm. e) Relative SERRS intensities 725 cm^{-1} recorded at 0, 5, 15 and 24h of incubation with the highest hemin concentration (150 µM), error bars refer to standard deviation of three different measurements. All measurements were acquired with an excitation laser wavelength of 785 nm, 10× objective, and a laser power of 115.95 kW cm^{-2} for 10 s.

3. Conclusions

The present study demonstrates the application of surface-enhanced Raman scattering to the detection of extracellular tumor metabolites under diverse cell culture conditions. IDO-1 activity in tumor cells was monitored by SERS, measuring simultaneously extracellular changes in both the substrate and the product of the enzymatic activity (Trp and Kyn, respectively). By using highly efficient nanostructured plasmonic substrates we were able to estimate by SERS the Kyn/Trp ratio, which is well known to correlate with bad prognosis in cancer patients. On the other hand, we observed that the cofactor of IDO-1 enzyme, hemin, affects the SERS profile in a dose-dependent manner and this SERS signal was further associated with the induction of cell death at toxic concentrations of hemin. Additionally, we observed that the levels of purine derivative metabolites were directly related to cell death induction, working as a suitable biomarker of cell death. Finally, the reported approach provided an additional tool for the spatial-temporal analysis of metabolite alterations and their response under different conditions. We demonstrated that these label-free studies can be extended to *in situ* imaging of metabolite exchange in tumor microenvironments, without disturbing the samples under investigation. This sensitive and cost-effective plasmonic substrate was effectively combined with 3D cell culture models, which more closely recreate the biochemical and biophysical factors in the tumor microenvironment, toward a real time imaging of heterogeneous metabolic alterations and cytotoxic effects on tumor cells, which will have important significance in diagnosis and therapy. Additionally, the development of standardized protocols and data processing programs for multiple metabolite quantification in complex environments appears as a crucial advancement to extend these SERS based metabolomics studies to a greater variety of metabolites from different diseases *in vivo*.

4. Experimental Section

Materials: Hexadecyltrimethylammonium chloride (CTAC, 25% W/W), , L-ascorbic acid (≥99%), sodium hypochlorite solution (10−15% available chlorine), sodium borohydride (NaBH4, 99%), poly(ethylene glycol) methyl ether thiol (PEG-6K-SH, Mn = 6000 g/ mol), poly(diallyldimethylammonium chloride) (PDDA, average Mw 100 000−200 000), poly(acrylic acid sodium salt) (PAA, Mw 15 000), hydrogen peroxide (H2O2, 28%), sulfuric acid (H2SO4, 98%), ethanol (EtOH, 99.8%), commercial samples of kynurenine (25 mg), Tryptophan (1g), ATP (1g), adenosine (1g), adenine (1g) , Hypoxanthine (1g), Inosine (1g), IFN- ϒ and Staurosporine drug were supplied by Sigma-Aldrich. Hydrogen tetrachloroaurate trihydrate (HAuCl4·3H2O, ≥99.9%) from Alfa Aesar was employed without further purification Polydimethylsiloxane (Sylgard 184) was bought from Dow Corning. Water purified with a Milli-Q system was used in all experiments

Synthesis of Au Nanoparticles and fabrication of plasmonic substrates:

*LBL methodology***:** Citrate-stabilized Au NS (30 nm in diameter) were synthesized according to a previously reported seeded growth method.[47] The production of randomly deposited AuNP multilayers was based on the well-known layer-by-layer (LBL) assembly methodology. Following this protocol, glass slides were sequentially immersed in polyelectrolyte solutions of PDDA (1 mg/mL, 0.05 M NaCl), PAA (1 mg/mL, 0.05 M NaCl), and (PDDA 1 mg/mL, 0.05 M NaCl) for 15 min. AuNP layers were then formed by immersing the polyelectrolyte-coated glass slides in a 0.9 mM AuNP solution for at least 3 h, followed by rising with water and drying under nitrogen flow. For the deposition of a second and third AuNP layers, the same procedure described above was repeated.

Template assisted self-assembly: All nanostructured substrates were prepared on glass coverslips (Menzel-Gläser, Nr 1.5) pre-cleaned with a dilute solution of Helmanex III. Au nanospheres were synthesized and functionalized with poly(ethylene glycol) methyl ether thiol 6000 average molar mass (PEG-6K-SH, Sigma-Aldrich), by adding 1 mg of PEG-6K-

SH per mL of 5 mM solution of AuNSs, following a previously reported seed mediated approach.[48] An optimized cleaning procedure was required prior to the SERS measurements. To this end, the nanoparticle assemblies were treated first with oxygen plasma (Diener PICO, 0.4 mbar O2, 200 W) and then exposed to UV−O_3 treatment. We observed that these cleaning treatments may alter the final SERS results, so it is crucial to optimize the exposure time and check the absorbance spectra of the substrate before and after cleaning (**Figure S22**).

Cell culture: HeLa cells were cultured using DMEM medium supplemented with 10% fetal calf serum (FCS). Cells were passaged or used for experiments when they reached 80% confluence. HeLa cells were harvested in a 12 well plate at the concentration of 6×10^4 cell/mL

Induction of IDO-1 enzyme expression in HeLa cells: In order to control the activation of IDO-1 in HeLa cells, we harvested HeLa cells in the presence or in the absence of IFN-ϒ (100ng/mL) for 48 hours. This activation process has been reported to correlate with the expression of high amounts of IDO protein.[49] As soon as the activation process finished, the cell media was exchanged and defined concentrations of diverse metabolites were added. This cell media contained varying concentrations of Trp depending on the cell experiment, 10 µM of Hemin, 2% FCS and 20% of DMEM diluted in HBBS buffer (hank´s balanced salt solution). After 24 h of cell culture under these conditions, the cell supernatant was collected and measured by SERS.

Q-RT_PCR: With the aim of studying the IDO-1 induction by IFN-ϒ activation, we harvested HeLa cells in the presence or the absence of IFN-ϒ (100ng/mL) for 72 hours. RNA was extracted using NucleoSpin® RNA isolation kit from Macherey-Nagel (Ref: 740955.240C). 1 µg of total RNA was used for cDNA synthesis using qScript cDNA Supermix from Quanta (Ref: 95048). Quantitative Real Time PCR (qRTPCR) was performed as previously described.[50] Universal Probe Library (Roche) primers and probes employed

are: For: gtgtttcaccaaatccacga, Rv: ctgatagctgggggttgc; probe: 20. All qRTPCR data presented were normalized using GAPDH (Hs 02758991_g1 from Applied Biosystems).

Stress condition cell assays: Cells were first harvested in a 12 well plate, at the concentration of 6×10^4 cell/mL and let 24 h for cell attachment. Consecutively, cell media was exchanged to recreate the stress conditions. We added 50 µM of H_2O_2 or 5 µM of Staurosporine drug to a control cell medium containing 2% FCS and 20% of DMEM diluted in HBBS buffer (hank´s balanced salt solution) or to a starvation medium not containing amino acids, such as HBBS buffer.). After 24 h of cell culture under these conditions, the cell supernatant was collected, centrifuged (3500 r.p.m, 5 min) and measured by SERS.

SERS measurements: Cell supernatant derived from different biological assays was sampled and 100 µL of the liquid was deposited on a plasmonic substrate surrounded using a hydrophobic pen (sigma), which prevented from liquid spreading. All biological studies were performed in three independent cell assays, which were spiked on three independent plasmonic substrates. Finally, SERS spectra were recorded under a 785 nm laser line, obtaining bands characteristic of metabolite vibrations. As a rule, 25 points from different substrate areas were measured every time. For data processing, we removed the background of SERS spectra following a polynomial curve and obtained the average spectrum of the 25 points for each condition by using Renishaw's WiRE software. Then, we identified the characteristic bands of the molecules of interest (Trp 760 cm^{-1}, Kyn 560 cm^{-1}, HX 725 cm^{-1}) and acquired their intensities. In Figure 2, the Ratio between kynurenine and tryptophan (760 cm^{-1}) was calculated as the division between the intensities at Kyn 560 cm^{-1} and Trp 760 cm^{-1} Mean ± SD values were calculated from the three independent cell assays. SERS mapping demonstrated the SERS enhancing ability of the organized discrete Au nanosphere assemblies in the nanostructured substrate (**Figure S2**).

Cell viability assay: Cells were seeded at a density of 6×10^4 cell/mL in 12 well plates and let 24 h for cell attachment. Subsequently, cell media was exchanged to recreate stress conditions,

varying either hemin or staurosporine concentrations. After 24 hours, cells were fixed in formalin (1mL/well) and washed with PBS. We then added 0.5 mL of 0.1% crystal violet, which bound to the cells in 20% methanol. The plate was cleaned with DI-water and crystal violet interacting with the cells was resuspended in 10% acetic acid. Finally, this volume was transferred to a spectrophotometer cuvette, to measure the absorbance at 595 nm, which correlates with the number of live cells.

HPLC: Kynurenine and Tryptophan samples separation was performed in reversed-phase chromatography using an ACQUITY UPLC BEH C18 1.7µm (2.1x100 mm) column (Waters, Manchester, UK) which was maintained at 30 ºC. For Hypoxanthine and Inosine ACQUITY UPLC BEH Amide 1.7 µm (2.1x50 mm) columns were used. The injected sample volume in all cases was 10 µL and the autosampler was set at 4 ºC. For Kynurenine and Tryptophan, the mobile phase was designed as phase A, consisting of a mixture of 0.1% formic acid-H_2O and phase B, ACN. The method used a gradient at constant flow rate (0.3 mL/min) combining solvent A and solvent B, programmed as follows: 0-0.5 min, linear change from A–B (95:5 v/v) to A–B (1:99 v/v) in 2.5 min and finally returning to 95% A at 3.7 min for column re-equilibration, which was completed at 5 min. For Hypoxanthine and Inosine the same mobile phase was used at 0.5mL/min with the following gradient: 0-0.5 min, linear change from A–B (5:95 v/v) to A–B (50:50 v/v) in 2.5 min and finally returning to 5% A at 4.1 min. The peaks were characterized by comparing the retention time and UV-vis absorbance at λ=363nm for Kynurenine, λ=277nm for Tryptophan and λ=249 for Hypoxanthine and Inosine.

Cancer-on-a-chip assays: To print the cancer-on-a-chip device, silicone ink was prepared using an elastomer base (Shin-Etsu Silicone) with curing agent at a 10:1 volume ratio and the mixture was loaded into a 10-mL clear syringe (PSY-E; Musashi Engineering, Ltd.) and printed with a diameter of 2 cm by a multi-headed 3D Discovery bioprinter (RegenHU, Switzerland) on a glass micro slide (26x76 mm). HeLa cells were seeded into collagen-based hydrogels, 3 mg/mL of collagen final concentration, after sequential trypsinization and

centrifugation. Consecutively, 80 µL of the mixture formed by cells with collagen solution were laden inside the silicon chamber, the gel-filled devices were then placed in prepared humid chambers in a CO_2 incubator, to allow collagen to polymerize at 37 °C for 20 min. We next added the cell media (2% FCS and 20% of DMEM diluted in HBBS buffer) with different Staurosporine/hemin concentrations and incubated the samples for 24 hours. The cell device was then assembled with the plasmonic substrate, placing the gold nanoparticle assembly directly in contact with the extracellular milieu. All non-commercial substrates were thoroughly cleaned and exposed to UV lamp for 20 minutes, to reduce the risk of biological contamination. Finally, the plasmonic substrate was illuminated with a 785 nm laser to record SERS spectra. For cell viability imaging, cells were incubated with Cytocalcalcein for 30 minutes, and the samples were then washed 3 times with 1xPBS and imaged with a Cell Axio Observer Microscope.

Supporting Information Supporting Information is available from the Wiley Online Library or from the author.

Acknowledgements

J. Plou acknowledges an FPU fellowship from the Spanish Ministry of Science, Innovation and Universities. L.M. Liz-Marzán acknowledges funding from the European Research Council (ERC AdG 787510, 4DbioSERS) and the Maria de Maeztu Units of Excellence Program from the Spanish State Research Agency (Grant No. MDM-2017-0720). C. García-Astrain acknowledges a Juan de la Cierva Fellowship from the Spanish Ministry of Science, Innovation and Universities (FJCI-2016-28887). We thank Dr. J. Calvo, and Dr. D. Otaegui at CIC biomaGUNE for support with LC/ESI-HRMS measurements. The work of A. Carracedo is supported by the Basque Department of Industry, Tourism and Trade (Elkartek) and the department of education (IKERTALDE IT1106-16, also participated by A. Gomez-Muñoz), the BBVA foundation, the MINECO (SAF2016-79381-R (FEDER/EU); Severo Ochoa Excellence Program SEV-2016-0644-18-1; Excellence Networks SAF2016-81975-REDT), European Training Networks Project (H2020-MSCA-ITN-308 2016 721532), the AECC (IDEAS175CARR, GCTRA18006CARR), La Caixa Foundation (HR17-00094) and the European Research Council (Starting Grant 336343, PoC 754627). CIBERONC was co-funded with FEDER funds and funded by ISCIII. A. Mihi acknowledges funding from the European Research Council (ERC StG 637116) and the Spanish Ministry of Science, Innovation and Universities for the excellence program SEV-2015-0496.

Received: ((will be filled in by the editorial staff))
Revised: ((will be filled in by the editorial staff))
Published online: ((will be filled in by the editorial staff))

References

[1] C. A. Lyssiotis, A. C. Kimmelman, *Trends Cell Biol.* **2017**, *27*, 863.
[2] U. E. Martinez-Outschoorn, M. Peiris-Pagés, R. G. Pestell, F. Sotgia, M. P. Lisanti, *Nat. Rev. Clin. Oncol.* **2017**, *14*, 11.
[3] A. Arruabarrena-Aristorena, A. Zabala-Letona, A. Carracedo, *Sci. Adv.* **2018**, *4*, eaar2606.
[4] B. Wegiel, M. Vuerich, S. Daneshmandi, P. Seth, *Front. Oncol.* **2018**, *8*, 284.
[5] H. Wang, F. Franco, P. C. Ho, *Trends in Cancer* **2017**, *3*, 583.
[6] P. J. Murray, *Nat. Immunol.* **2016**, *17*, 132.
[7] D. Anastasiou, *Br. J. Cancer* **2017**, *116*, 277.
[8] F. Yamazaki, R. Kid, *J. Biol. Chem.* **1988**, *263*, 2041.
[9] S. Yong, S. Lau *J, Chromatogr.* **1979**, *175*, 343.
[10] A. S. Edison, J. L. Markley, R. Bru, H. R. Eghbalnia, R. Powers, D. Raftery, D. S. Wishart, *Curr. Opin. Biotechnol.* **2017**, *43*, 34.
[11] W. Lu, X. Su, M. S. Klein, I. A. Lewis, O. Fiehn, J. D. Rabinowitz, *Annu. Rev. Biochem.* **2017**, 277.
[12] V. Ntziachristos, M. A. Pleitez, S. Aime, K. M. Brindle, *Cell Metab.* **2019**, *29*, 518.
[13] J. Langer, D. Jimenez de Aberasturi, J. Aizpurua, R. A. Alvarez-puebla, B. Auguie, J. J. Baumberg, G. C. Bazan, S. E. J. Bell, A. Boisen, A.G Brolo, J. Choo, D. Cialla-May, V. Deckert, L. Fabris, K. Faulds, F.J García de Abajo, R. Goodacre, D. Graham, A.J Haes, C.L Haynes. C. Huck, S.A Maier, T. Mayerhöfer, M. Moskovits, K. Murakoshi, J.M Nam, S. Nie, Y. Ozaki, I. Pastoriza-Santos, J. Perez-Juste. J. Popp, A. Pucci, S. Reich, B. Ren, G.C. Schatz, T. Shegai, S. Schlücker, L.L Tay, K.G. Thomas, Z.Q Tian, R.P Van Duyne, T. Vo-Dinh, Y. Wang, K.A Willets, C. Xu, H. Xu, Y. Xu, Y.S Yamamoto, B. Zhao, L.M. Liz-Marzán. *ACS Nano* **2020**, *14*, 28.
[14] G. Bodelón, V. Montes-García, V. López-Puente, E. H. Hill, C. Hamon, M. N. Sanz-Ortiz, S. Rodal-Cedeira, C. Costas, S. Celiksoy, I. Pérez-Juste, L. Scarabelli, A. La Porta, J. Pérez-Juste, I. Pastoriza-Santos, L.M. Liz-Marzán, *Nat. Mater.* **2016**, *15*, 1203.
[15] N. Feliu, M. Hassan, E. Garcia Rico, D. Cui, W. J. Parak, R. A Alvarez-Puebla, *Langmuir* **2017**, *38*, 9711.
[16] B. Kang, L. A. Austin, M. A. El-sayed, *ACS Nano* **2014**, *8*, 4883.
[17] D. Lin, J. Pan, H. Huang, G. Chen, S. Qiu, H. Shi, W. Chen, Y. Yu, S. Feng, R Chen, *Sci. Rep.* **2014**, *4*, 4751.
[18] C. Yorucu, K. Lau, S. Mittar, N. H. Green, A. Raza, I. U. Rehman, S. MacNeil, *Appl. Spectrosc. Rev.* **2016**, *51*, 243.
[19] V. Shalabaeva, L. Lovato, R. La Rocca, G. C. Messina, M. Dipalo, E. Miele, M. Perrone, F. Gentile, F. De Angelis, *PLoS One* **2017**, *12*, e0175581.
[20] M. Hassoun, I.W. Schie, T. Tolstik, S. E. Stanca, C. Krafft, J. Popp, *Beilstein J. Nanotechnol.* **2017**, *8*, 1183.
[21] F. Lussier, D. Missirlis, J. P. Spatz, J. F. Masson, *ACS Nano* **2019**, *13*, 1403.
[22] F. Lussier, T. Brulé, M. Vishwakarma, T. Das, J. P. Spatz, J. F. Masson, *Nano Lett.* **2016**, *16*, 3866.
[23] K. Renner, K. Singer, G. E. Koehl, E. K. Geissler, K. Peter, P. J. Siska, M. Kreutz, *Front. Immunol.* **2017**, *8*, 248.

[24] K. Singer, W.-C. Cheng, M. Kreutz, P.-C. Ho, P. J. Siska, *Dis. Model. Mech.* **2018**, *11*, dmm034272.
[25] G. Bodelón, V. Montes-García, C. Costas, I. Pérez-Juste, J. Pérez-Juste, I. Pastoriza-Santos, L. M. Liz-Marzán, *ACS Nano* **2017**, *11*, 4631.
[26] C. Hanske, E. H. Hill, D. Vila-Liarte, G. González-Rubio, C. Matricardi, A. Mihi, L. M. Liz-Marzán, *ACS Appl. Mater. Interfaces* **2019**, *11*, 11763.
[27] C. Matricardi, C. Hanske, J. L. Garcia-Pomar, J. Langer, A. Mihi, L. M. Liz-Marzán, *ACS Nano* **2018**, *12*, 8531.
[28] S. Nie, C. G. Castillo, K. L. Bergbauer, J. F. R. Kuck, I. R. Nabiev, N. T. Yu, *Appl. Spectrosc.* **1990**, *44*, 571.
[29] Q. Tu, J. Eisen, C. Chang, *J. Biomed. Opt.* **2010**, *15*, 20512.
[30] S. S. De Ravin, K. A. Zarember, D. Long-Priel, K. C. Chan, S. D. Fox, J. I. Gallin, D. B. Kuhns, H. L. Malech, *Blood* **2010**, *116*, 1755.
[31] J. E. Cheong, L. Sun, *Trends Pharmacol. Sci.* **2018**, *39*, 307.
[32] N. T. Nguyen, A. Kimura, T. Nakahama, I. Chinen, K. Masuda, K. Nohara, Y. Fujii-Kuriyama, T. Kishimoto, *Proc. Natl. Acad. Sci.* **2010**, *107*, 19961.
[33] E. Lenzi, D. Jimenez de Aberasturi, L. M. Liz-Marzán, *ACS Sens.* **2019**, *4*, 1126.
[34] W. Däubener, N. Wanagat, K. Pilz, S. Seghrouchni, H. G. Fischer, U. J. Hadding, *Immunol. Methods* **1994**, *168*, 39.
[35] M. T. Nelp, P. A. Kates, J. T. Hunt, J. A. Newitt, A. Balog, D. Maley, X. Zhu, L. Abell, A. Allentoff, R. Borzilleri, H.A. Lewis, Z. Linz, S.P. Seitz, C. Yanz, J.T Groves. *Proc. Natl. Acad. Sci.* **2018**, *115*, 3249.
[36] J. Basran, I. Efimov, N. Chauhan, S. J. Thackray, J. L. Krupa, G. Eaton, G. A. Griffith, C. G. Mowat, S. Handa, E. L. Raven, *J. Am. Chem. Soc.* **2011**, *133*, 16251.
[37] W. R. Premasiri, J. C. Lee, A. Sauer-budge, R. Théberge, C. E. Costello, L. D. Ziegler, *Anal. Bioanal. Chem.* **2016**, *408*, 4631.
[38] S. Chiang, S. Chen, L. Chang, *Int. J. Mol. Sci.* **2019**, *20*, 1.
[39] L. Antonioli, C. Blandizzi, P. Pacher, G. Haskó, *Nat. Rev. Cancer* **2013**, *13*, 842.
[40] F. Di Virgilio, E. Adinolfi, *Oncogene* **2017**, *36*, 293.
[41] Y. J. Wang, R. Fletcher, J. Yu, L. Zhang, *Genes Dis.* **2018**, *5*, 194.
[42] C. Hernandez, P. Huebener, R. F. Schwabe, *Oncogene* **2016**, *35*, 5931.
[43] S. W. Y. Chiu, H. W. Cheng, Z. X. Chen, H. H. Wang, M. Y. Lai, J. K. Wang, Y. L. Wang, *Phys. Chem. Chem. Phys.* **2018**, *20*, 8032.
[44] J. Kabir, M. Lobo, I. Zachary, *Biochem. J.* **2002**, *367*, 145.
[45] H. Yi, Y. H. Jeong, Y. Kim, Y. Choi, H. E. Moon, D. Cho, *Nat. Biomed. Eng.* **2019**, *3*, 509.
[46] J. Yu, E. Berthier, A. Craig, , T. E. de Groot, S. Sparks, P. N. Ingram, D. F. Jarrard, W. Huang, D. J. Beebe, A. B. Theberge, *Nat. Biomed. Eng.* **2019**, *3*, 830.
[47] N. G. Bastús, J. Comenge, V. Puntes, *Langmuir* **2011**, *27*, 11098.
[48] C. Hanske, G. González-Rubio, C. Hamon, P. Formentín, E. Modin, A. Chuvilin, A. Guerrero-Martínez, L. F. Marsal, L. M. Liz-Marzán, *J. Phys. Chem. C* **2017**, *121*, 10899.
[49] B. Jürgens, U. Hainz, D. Fuchs, T. Felzmann, A. Heitger, *Blood*, **2009**, *114*, 3235.
[50] V. Torrano, L. Valcarcel-Jimenez, A. R. Cortazar, X. Liu, J. Urosevic, M. Castillo-Martin; S. Fernández-Ruiz, G. Morciano, , A. Caro-Maldonado, M. Guiu, P. Zuñiga-García, M. Graupera, A. Bellmunt, P. Pandya, M. Lorente, N. Martín-Martín, J.D Sutherland, P. Sanchez-Mosquera, L. Bozal-Basterra, A.Zabala-Letona, A. Arruabarrena-Aristorena, A. Berenguer, N. Embade, A. Ugalde-Olano, I. Lacasa-Viscasillas, A. Loizaga-Iriarte, M. Unda-Urzaiz, N. Schultz, A.M. Aransay, V. Sabz-Moreno, R. Barrio, G. Velasco, P. Pinton, C. Cordon-Cardo, J.W Locasale, R.R Gomis, A. Carracedo. *Nat. Cell Biol.* **2016**, *18*, 645.

Surface-enhanced Raman Scattering is used to monitor metabolic perturbations in tumor extracellular environment in a label-free and non-invasive manner, providing new readouts in the secretion of kynurenine, tryptophan and purine derivative metabolites by cancer cells.

Javier Plou[1,2,3], Isabel García[1,2,] Mathias Charconnet[1,4], Ianire Astobiza[3,5,] Clara García-Astrain[1], Cristiano Matricardi[6], Agustín Mihi[6], Arkaitz Carracedo[3,5,7,8], Luis M. Liz-Marzán[1,2,8*]

Multiplex SERS Detection of Metabolic Alterations in Tumor Extracellular Media

ToC image